Journal of Computational and Applied Mathematics 42 (1992) 137–155
North-Holland

CAM 1187

The electromagnetic inverse problem in the time domain for a dissipative slab and a point source using invariant imbedding: Reconstruction of the permittivity and conductivity

Sailing He and Staffan Ström

Division of Electromagnetic Theory, Royal Institute of Technology, Stockholm, Sweden

Received 11 February 1991
Revised 24 May 1991

Abstract

He, S. and S. Ström, The electromagnetic inverse problem in the time domain for a dissipative slab and a point source using invariant imbedding: Reconstruction of the permittivity and conductivity, Journal of Computational and Applied Mathematics 42 (1992) 137–155.

We consider the electromagnetic inverse problem for a point source above an inhomogeneous dissipative slab of permittivity $\epsilon(z)$ and conductivity $\sigma(z)$, where z is the depth. Two inversion algorithms based on the invariant imbedding equations derived in previous work are used to reconstruct both the permittivity and the conductivity. Both algorithms use two-sided reflection data and one of them also uses transmission data. Results are presented for clean and noisy data.

Keywords: Wave splitting, invariant imbedding, inverse scattering, dissipative stratified media, reconstruction of permittivity and conductivity.

1. Introduction

The problem of reconstructing the physical properties of a stratified medium from scattered field data has received considerable attention and both time- and frequency-domain methods have been used (see, e.g., [2,9,16,17] and earlier references given there). In the present paper we consider the case of a transient point source above an inhomogeneous slab in which the permittivity $\epsilon(z)$ and conductivity $\sigma(z)$ vary with the depth z. The inverse problem of reconstructing these two functions from measured data on the slab surfaces is solved by means

Correspondence to: Prof. S. Ström, Division of Electromagnetic Theory, Royal Institute of Technology, 100 44 Stockholm, Sweden.

of two inversion algorithms based on invariant imbedding equations for this scattering problem which have been derived in a previous paper [8]. In [8] it is shown that by means of a Hankel transform and an additional appropriately chosen transformation, the problem can be formulated in terms of imbedding equations which are closely analogous to the imbedding equations for plane wave normal incidence on a slab of this kind (see [9–12]). As a consequence, inversion algorithms analogous to those considered in [10–12] can be applied to the present formulation of the point source case. In particular it is noted that the "extension of data" property, which was found for the normal incidence case [9], can be exploited also in the present formulation of the point source case.

The present paper is organized as follows. In Section 2 we give a summary of those results from [8] which are most relevant for the inverse aspect and in Section 3 we derive some additional properties of the scattering kernels which lead to the extension of data property. In Section 4 we describe an inversion algorithm that uses two-sided reflection data as well as transmission data. An iterative inversion algorithm for which two-sided reflection data suffice is given in Section 5. In Section 6 we illustrate the numerical performance of the inversion algorithms for clean and noisy synthetic data.

2. Summary of some previous results

The imbedding equations and jump relations for the various scattering kernels that describe the scattering of a (vertical magnetic dipole) point source field from an inhomogeneous slab are derived in [8]. In this section we summarize those relations which will be needed in the inversion algorithms. As described in [8], the scattering problem is formulated and solved in terms of a set of transformed "nonphysical" scattering kernels $R_1^{\pm}$, $T_1^{\pm}$, $V_1^{\pm}$, $W_1^{\pm}$, where the superscripts refer to incidence from a point source above (+) and below (−) the slab, respectively. The geometry of the problem is described in Fig. 1.

The Hertz potential $U(r, z, t)$ of the magnetic dipole is Hankel-transformed according to

$$u(\kappa, z, t) = \int_0^\infty U(r, z, t) J_0(\kappa r) r \, \mathrm{d}r, \tag{1}$$

and the inverse problem is solved for $u(\kappa, z, t)$ (r is the radius in a cylindrical coordinate system (r, φ, z)). The dependence on the Hankel-transformed functions on the parameter κ will be suppressed in the sequel, i.e., we write $u(\kappa, z, t) \equiv u(z, t)$, etc. We consider, for arbitrary z, the splitting

$$u_1^+ = \tfrac{1}{2}\left[u - c(z)\, \partial_t^{-1} u_z\right], \tag{2}$$

$$u_1^- = \tfrac{1}{2}\left[u + c(z)\, \partial_t^{-1} u_z\right], \tag{3}$$

where $\partial_t^{-1} f \equiv \int_0^t f(t')\, \mathrm{d}t'$, and $c = c_0 = (\epsilon_0 \mu_0)^{-1/2}$ for $z < 0$, $c = c_1 = (\epsilon_1 \mu_0)^{-1/2}$ for $z > L$. It is convenient to change to the travel time coordinates

$$x(z) = \frac{1}{l} \int_0^z \sqrt{\epsilon(z')\mu_0}\, \mathrm{d}z', \tag{4}$$

$$s = t/l, \tag{5}$$

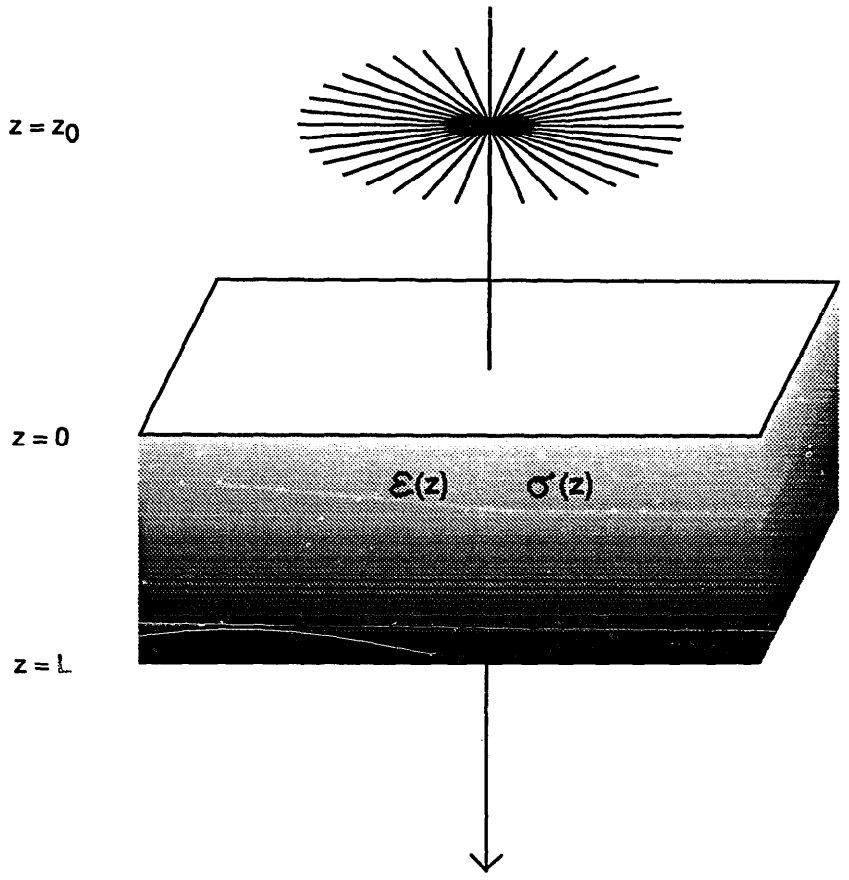

Fig. 1. The scattering configuration.

and with $u(z, t) \equiv w(x, s)$, the wave equations and boundary conditions become

$$w_{xx} - w_{ss} + A(x)w_x + B(x)w_s + C(x)w = 0, \quad 0 < x < 1, \tag{6}$$

$$w_{xx} - w_{ss} - \kappa^2 c_0^2 l^2 w = 0, \quad x < 0, \ x \neq x_0, \tag{7}$$

$$w_{xx} - w_{ss} - \kappa^2 c_1^2 l^2 w = 0, \quad x > 1, \tag{8}$$

w, w_x are continuous at $x = 0, 1$,

where

$$A(x) = -\frac{\mathrm{d}}{\mathrm{d}x} \ln c(z(x)), \tag{9}$$

$$B(x) = -l \frac{\sigma(z(x))}{\epsilon(z(x))}, \tag{10}$$

$$C(x) = -\kappa^2 c^2(z(x)) l^2. \tag{11}$$

In the new variables the splitting is given by

$$w_1^+ = \tfrac{1}{2}\left[w - \partial_s^{-1} w_x\right], \tag{12}$$

$$w_1^- = \tfrac{1}{2}\left[w + \partial_s^{-1} w_x\right]. \tag{13}$$

For down-going incidence the associated reflection and transmission kernels $R_1^+(0, 1, s)$ and $T_1^+(0, 1, s)$, respectively, are given by

$$w_1^-(0, s) = \int_0^s R_1^+(0, 1, s-s') w_1^+(0, s')\, ds', \tag{14}$$

$$w_1^+(1, s+1) = t^+(0, 1) w_1^+(0, s) + \int_0^s T_1^+(0, 1, s-s') w_1^+(0, s')\, ds', \tag{15}$$

where

$$t^+(0, 1) = \exp\left[-\frac{1}{2}\int_0^1 \{A(x) - B(x)\}\, dx\right]. \tag{16}$$

The analogous relations for up-going incidence are given in [8]. In the invariant imbedding approach (see, e.g., [3,5]) one considers also the corresponding kernels $R_1^\pm(x, y, s)$ and $T_1^\pm(x, y, s)$ for the subregion $[x, y]$, $0 < x < y < 1$. We refer to [8] for further details.

We note that other types of splittings have been considered, which may be said to be somewhat more physical in the present problem (cf. [6,7,15]). However, the motivation for our choice of formulation is that it can be developed as a generalization of the plane wave normal incidence case and that it provides a solution of the inverse scattering problem in which the permittivity $\epsilon(z)$ and conductivity $\sigma(z)$ can be reconstructed simultaneously. Furthermore, the imbedding equations are simpler in the present formulation (cf. [6,7]). It should also be mentioned that the reflection or transmission kernels in the two different formulations are related through a Volterra equation of the second kind, which allows an accurate computation of the physical kernels from the nonphysical ones and vice versa (cf. [8]).

The imbedding equations, initial values and boundary values of the reflection kernels $R_1^\pm(x, y, s)$ for the subregion $[x, y]$ are [8]

$$R_{1x}^+(x, y, s) = 2R_{1s}^+ - B(x)R_1^+ - \tfrac{1}{2}[A(x) + B(x)]R_1^+ * R_1^+ + R_0^{x+}, \quad s > 0, \tag{17}$$

$$R_1^+(x, y, 0^+) = -\tfrac{1}{4}[A(x) - B(x)], \quad x < y, \tag{18}$$

$$R_1^+(y, y, s) = -2\frac{1}{s} J_2\left(\sqrt{-C(y)}\, s\right) = -2\frac{1}{s} J_2(\kappa c(y) l s), \quad s > 0, \tag{19}$$

where

$$R_0^{x+} = -\tfrac{1}{2} C(x)\{1 + 2 * R_1^+ + 1 * R_1^+ * R_1^+\} \tag{20}$$

(the star $*$ denotes a time convolution) and

$$R_{1y}^-(x, y, s) = -2R_{1s}^- + B(y)R_1^- - \tfrac{1}{2}[A(y) - B(y)]R_1^- * R_1^- + R_0^{y-}, \quad s > 0, \tag{21}$$

$$R_1^-(x, y, 0^+) = \tfrac{1}{4}[A(y) + B(y)], \quad x < y, \tag{22}$$

$$R_1^-(x, x, s) = -2\frac{1}{s} J_2(\kappa c(x) l s), \quad s > 0, \tag{23}$$

where

$$R_0^{y-} = \tfrac{1}{2}C(y)\{1 + 2 * R^{-1} + 1 * R_1^- * R_1^-\}. \tag{24}$$

These kernels are discontinuous across the plane $s = 2(y-x)$, where they have the following jumps:

$$R_1^+(x, y, s)|_{s=2(y-x)^-}^{s=2(y-x)^+} = \tfrac{1}{4}[A(y) - B(y)] \exp\left[\int_x^y B(x')\,dx'\right], \tag{25}$$

$$R_1^-(x, y, s)|_{s=2(y-x)^-}^{s=2(y-x)^+} = -\tfrac{1}{4}[A(x) + B(x)] \exp\left[\int_x^y B(x')\,dx'\right]. \tag{26}$$

For times less than one round trip through the subregion $[x, y]$, the position of the rear interface has no effect on $R_1^{\pm}(x, y, s)$. Thus

$$R_1^+(x, y, s) = R_1^+\left(x, x + \left(\tfrac{1}{2}s\right)^+, s\right), \quad s < 2(y-x), \tag{27}$$

$$R_1^-(x, y, s) = R_1^-\left(y - \left(\tfrac{1}{2}s\right)^+, y, s\right), \quad s < 2(y-x). \tag{28}$$

The transmission kernels $T_1(x, y, s)$ (cf. [8, Eq. (111)]) and its resolvent $W_1(x, y, s)$ satisfy the equation

$$T_1(x, y, s) + W_1(x, y, s) + \int_0^s T_1(x, y, s-s')W_1(x, y, s')\,ds' = 0. \tag{29}$$

The imbedding equation for W_1 is

$$W_{1x}(x, y, s) = \tfrac{1}{2}[A(x) + B(x)]\{R_1^+ + R_1^+ * W_1\} + W_0^x, \quad s > 0, \tag{30}$$

where

$$W_0^x = \tfrac{1}{2}C(x)\{1 + 1 * R_1^+ + 1 * W_1 + 1 * R_1^+ * W_1\}. \tag{31}$$

The kernels $V_1^{\pm}(x, y, s)$ satisfy

$$R_1^{\pm}(x, y, s) = V_1^{\pm}(x, y, s) + \int_0^s T_1(x, y, s-s')V_1^{\pm}(x, y, s')\,ds' \tag{32}$$

and

$$V_1^{\pm}(x, y, s) = R_1^{\pm}(x, y, s) + \int_0^s R_1^{\pm}(x, y, s-s')W_1(x, y, s')\,ds'. \tag{33}$$

The measured values of the total field for $0 \leqslant r < \infty$, $z = 0$ determine the Hertz potential $U(r, 0, t)$. In the inverse problem, we first choose a fixed κ in the Hankel transform (1). From the (nonphysical) splitting given by (2) and (3), the reflection and transmission kernels $R_1^{\pm}$ and $T_1^{\pm}$ are determined according to (14) and (15) and the corresponding equations for up-going incidence, and the inversion will be carried out for these Hankel-transformed quantities.

The permittivity $\epsilon(z)$ and conductivity $\sigma(z)$, which are the unknowns in the inverse problem, are related to the coefficients $A(x)$ and $B(x)$ in (6) through (cf. (9) and (10))

$$\epsilon(z(x)) = \epsilon_0 \exp\left[2\int_0^x A(x')\,dx'\right], \tag{34}$$

$$\sigma(z(x)) = -\frac{1}{l}\epsilon_0 B(x) \exp\left[2\int_0^x A(x')\,dx'\right], \tag{35}$$

where

$$z(x) = c_0 l \int_0^x \exp\left[-\int_0^{x'} A(x'')\,dx''\right] dx'. \tag{36}$$

The coefficient $C(x)$ in (6) is determined by $A(x)$ through (cf. (11))

$$C(x) = -\kappa^2 c_0^2 l^2 \exp\left[-2\int_0^x A(x')\,dx'\right]. \tag{37}$$

Thus, we consider $A(x)$ and $B(x)$ as our unknown functions and we need two additional independent relations between $A(x)$, $B(x)$ and $C(x)$ in order to reconstruct both the permittivity and the conductivity. Algorithms for this are given in Sections 4 and 5.

3. The extension of data property of $R_1^{\pm}$ and T_1

It has been shown that in the plane wave normal incidence case (which corresponds to $C(x) \equiv 0$) the kernels $W_1(x, y, s)$ and $V_1^{\pm}(x, y, s)$ vanish for $s > 2(y - x)$, i.e., after one round trip (cf. [9.14]). When $C(x) \not\equiv 0$, this is no longer the case, but one has the result that $W_1(x, y, s)$ and $V_1^{\pm}(x, y, s)$ are constants for $s > 2(y - x)$, cf. [13]. Here we derive this property for the whole slab, but the arguments can be applied to any subregion of the slab. The derivation follows closely the one given in [9, Appendix A], with only minor changes necessitated by the fact that now $C(x) \not\equiv 0$. Furthermore, we keep the assumption that $\epsilon(z)$ is continuous everywhere. In view of the above, our presentation is somewhat brief.

The solution w of (6) can be expressed in terms of transmission data $w_+^t(s)$ as [13]

$$\begin{aligned} w(x, s) &= w_+^i(x, s) + w_+^r(x, s) \\ &= [t^+(x, 1)]^{-1}\left\{w_+^t(s - x) + \frac{1}{2}\int_x^{2-x} w_+^t(s - s')N(x, s')\,ds'\right\}, \quad 0 < x < 1, \end{aligned} \tag{38}$$

where the function $N(x, s)$ satisfies

$$N_{xx} - N_{ss} + B(x)(N_x + N_s) + D(x)N = 0, \quad 0 < x < 1, \tag{39}$$

$$N(x, x) = \tfrac{1}{2}[B(1^-) - A(1^-)] - \int_x^1 D(s')\,ds', \tag{40}$$

$$N(x, 2 - x) = \tfrac{1}{2}[B(1^-) - A(1^-)] \exp\left[\int_x^1 B(s')\,ds'\right], \tag{41}$$

where

$$D(x) = C(x) + \tfrac{1}{4}(B^2 - A^2) + \tfrac{1}{2}(B' - A'). \tag{42}$$

Here the prime denotes differentiation with respect to x. Differentiating (38) with respect to x, setting $x = 0$ in the resulting equation and integrating this equation from 0 to s, we obtain

$$-w_+^{\mathrm{i}}(s) + w_+^{\mathrm{r}}(s) = -[t^+(0,1)]^{-1}\left\{w_+^{\mathrm{t}}(s) - \frac{1}{2}\int_0^s w_+^{\mathrm{t}}(s')F(s-s')\,\mathrm{d}s'\right\}, \tag{43}$$

where

$$F(s) = a + bH(s-2) + \int_0^s \left[N_x(0,s') - \tfrac{1}{2}(A-B)|_{0^+}N(0,s')\right]H(2-s')\,\mathrm{d}s', \tag{44}$$

and

$$a = -(A-B)|_{0^+} - N(0,0), \qquad b = -N(0,2),$$

$$H(s) = \begin{cases} 0, & \text{if } s < 0, \\ 1, & \text{if } s > 0. \end{cases}$$

The V_1^+ kernel can be expressed as

$$V_1^+(0,1,s) = -\tfrac{1}{4}[N(0,s)H(2-s) - F(s)]. \tag{45}$$

From (44) and (45), one can see that $V_1^+(0,1,s)$ is constant for $s > 2$. In order to determine this constant, consider

$$f(x) = \int_x^{2-x} \left[N_x(x,s') - \tfrac{1}{2}(A-B)N(x,s')\right]\mathrm{d}s'. \tag{46}$$

By considerations analogous to those given in [8, Appendix A] one finds

$$f(0) = k + \int_0^1 \left\{C(x)\left[\int_x^{2-x} N(x,s')\,\mathrm{d}s'\right]\exp\left[\frac{1}{2}\int_0^x [A(x') + B(x')]\,\mathrm{d}x'\right]\right\}\mathrm{d}x, \tag{47}$$

and

$$V_1^+(0,1,s) = \frac{1}{4}\int_0^1 \left\{C(x)\left[\int_x^{2-x} N(x,s')\,\mathrm{d}s'\right]\exp\left[\frac{1}{2}\int_0^x [A(x') + B(x')]\,\mathrm{d}x'\right]\right\}\mathrm{d}x, \quad s > 2, \tag{48}$$

which is a constant. Similarly,

$$V_1^-(0,1,s) = -W_1(0,1,s) = \frac{1}{4}\int_0^1 \left\{C(x)\left[\int_x^{2-x} N(x,s')\,\mathrm{d}s'\right]\exp\left[\frac{1}{2}\int_0^x [A(x') + B(x')]\,\mathrm{d}x'\right]\right\}\mathrm{d}x, \quad s > 2. \tag{49}$$

Thus, for $C(x) \equiv 0$ we have $f(0) = k$ and W_1 and $V_1^{\pm}$ have compact support, as in [9]. For the present case with $C(x) \not\equiv 0$ we have

$$W_0 \equiv W_1(0,1,s) = -V_1^{\pm}(0,1,s), \quad s > 2. \tag{50}$$

The property (50) is sufficient to establish the extension of data for $R_1^{\pm}$ and T_1. Again one can proceed in close analogy with the $C(x) \equiv 0$ case. From the resolvent equation (29), we can determine $W_1(0, 1, s)$, $0 < s < 2$, from one round trip transmission data, i.e., $T_1(0, 1, s)$, $0 < s < 2$. Since $W_1(0, 1, s)$ is continuous, we obtain the constant W_0 by letting $s \to 2^-$ and thus $W_1(0, 1, s)$ is known for all s. For $s > 2$, (29) may be written

$$T_1(0, 1, s) + W_0 + \int_0^2 T_1(0, 1, s')W_1(0, 1, s - s')\, ds'$$

$$+ \int_2^s T_1(0, 1, s')W_1(0, 1, s - s')\, ds' = 0. \tag{51}$$

In the first integral in (51) we have $0 < s' < 2$, i.e., this integral is a known function of s. In the second integral we have $2 < s' < s$. i.e., for $s > 2$ (51) is an integral equation for $T_1(0, 1, s)$, $s > 2$, from which this function can be determined. Thus $T_1(0, 1, s)$ for $0 < s < 2$ determines $T_1(0, 1, s)$ for all s (extension of data).

This result can now be used in (32) to obtain the corresponding property for $R_1^{\pm}(0, 1, s)$. For $s > 2$ we have from (32) and (50)

$$R_1^{\pm}(0, 1, s) = V_1^{\pm}(0, 1, s) + \int_0^s T_1(0, 1, s - s')V_1^{\pm}(0, 1, s')\, ds'$$

$$= -W_0 - W_0 \int_2^s T_1(0, 1, s - s')\, ds' + \int_0^2 T_1(0, 1, s - s')V_1^{\pm}(0, 1, s')\, ds'. \tag{52}$$

The first integral in (52) is a known function of s and in the second integral $V_1^{\pm}(0, 1, s)$ is determined from knowledge of $R_1^{\pm}(0, 1, s)$ and $W_1(0, 1, s)$ for $0 < s < 2$ according to (33), and thus $R_1^{\pm}(0, 1, s)$ for $s > 2$ is determined by the same data. Therefore, all the information concerning the reflected and transmitted field is contained in one round trip reflection and transmission data for $R_1^{\pm}$ and T_1.

4. Inversion based on reflection and transmission data

We shall consider two inversion algorithms which both are patterned on the treatment given in [10] for the plane wave normal incidence case. The first of them, which uses both reflection and transmission data, will be discussed in this section. We indicate how the previously derived equations can be exploited to arrive at the required two independent relations for $A(x)$ and $B(x)$ in terms of scattering data.

We note that the extension of data concerning the travel time coordinate s given in Section 3 can be applied to any subregion $[x, y]$ so that we have

$$V_1^{\pm}(x, y, s) = -W_1(x, y, s) = -W_1(x, y, 2(y - x)), \quad s > 2(y - x). \tag{53}$$

Here we should notice that $W_1(x, y, s)$ and $T_1(x, y, s)$ are continuous functions, but

$V_1^{\pm}(x, y, s)$ and $R_1^{\pm}(x, y, s)$ have a jump at $s = 2(y-x)$. Therefore, we write (32) for $y = 1$ more explicitly as

$$R_1^-(x, 1, s) = -W_1(x, 1, 2(1-x)) + \int_0^{2(1-x)} T_1(x, 1, s-s')V_1^-(x, 1, s')\,ds' - W_1(x, 1, 2(1-x))\int_{2(1-x)}^{s} T_1(x, 1, s-s')\,ds', \quad s > 2(1-x). \tag{54}$$

Setting $s = 2(1-x)^+$ in the above equation yields

$$R_1^-\big(x, 1, 2(1-x)^+\big) = -W_1(x, 1, 2(1-x)) + \int_0^{2(1-x)} T_1(x, 1, s-s')V_1^-(x, 1, s')\,ds'. \tag{55}$$

In (55) we introduce $V_1^{-1}(x, 1, s')$ as given by (33) and use (29) to obtain

$$R_1^-\big(x, 1, 2(1-x)^+\big) = -W_1(x, 1, 2(1-x)) - \int_0^{2(1-x)} W_1(x, 1, 2(1-x)-s')R_1^-(x, 1, s')\,ds'. \tag{56}$$

Using (28), we obtain the jump in R_1^- as

$$R_1^-(x, 1, s)\big|_{2(1-x)^-}^{2(1-x)^+} = -W_1(x, 1, 2(1-x)) - \int_0^{2(1-x)} W_1(x, 1, 2(1-x)-s')R_1^-(0, 1, s')\,ds' - R_1^-\big(0, 1, 2(1-x)^-\big), \tag{57}$$

and in view of (26) we thus have

$$\int_0^{2(1-x)} W_1(x, 1, 2(1-x)-s')R_1^-(0, 1, s')\,ds' + W_1(x, 1, 2(1-x)) + R_1^-\big(0, 1, 2(1-x)^-\big) = \tfrac{1}{4}[A(x)+B(x)]\exp\left[\int_x^1 B(x')\,dx'\right]. \tag{58}$$

From (18), we have

$$R_1^+(x, 1, 0^+) = -\tfrac{1}{4}[A(x)-B(x)]. \tag{59}$$

From the above it is seen that the following data are sufficient to reconstruct both $A(x)$ and $B(x)$:

$$R_1^+(0, 1, s), \quad 0<s<2, \qquad R_1^-(0, 1, s), \quad 0<s<2,$$
$$T_1(0, 1, s), \quad 0<s<2, \qquad G(1),$$

where

$$G(1) = \exp\left[-\int_0^1 B(x')\,dx'\right],$$

which is a measurable constant associated with the attenuation of the field within the slab.

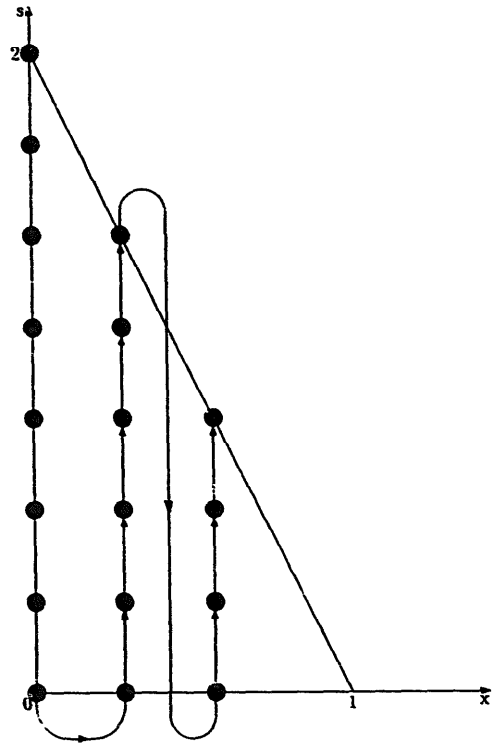

Fig. 2. The order in which the values of R_1^+ are determined when solving the inverse problem.

Assuming that a set of grid points in (x, s)-space has been established (cf. Fig. 2), the inversion algorithm for reconstructing $A(x)$ and $B(x)$ can now be described in terms of the following steps.

(1) Use (29) for $y = 1$ to determine $W_1(0, 1, s)$, $0 < s < 2$, from the known data $T_1(0, 1, s)$, $0 < s < 2$,

$$T_1(0, 1, s) + W_1(0, 1, s) + \int_0^s T_1(0, 1, s - s')W_1(0, 1, s')\, ds' = 0.$$

(2) Use (58) and (59) to determine starting values $A(0)$ and $B(0)$.

(3) Use $W_1(0, 1, s)$ and the known data $R_1^+(0, 1, s)$ to provide starting values for stepping W_1 forward in x according to (30) for $y = 1$.

(4) Use (17) for $y = 1$ for stepping R_1^+ forward in x at $s = 0$.

(5) Use (17) to step R_1^+ forward in s for the new x grid point.

This sequence of steps (2)–(5) can now be repeated to move one step deeper into the slab, and so on. Some numerical examples which illustrate the performance of this algorithm are discussed in Section 6.

5. An iterative inversion algorithm based on reflection data

In analogy with the one-dimensional case an iterative inversion algorithm can also be constructed (see [10]), which uses only reflection data for one round trip, i.e., $R_1^+(0, 1, s)$ and

$R_1^-(0, 1, s)$ for $0 < s < 2$. This iteration scheme is based on integrated versions of (17) and (21). From (17) with $y = 1$ we obtain

$$\begin{aligned} R_1^+(x, 1, s) &= R_1^+(0, 1, s+2x) \\ &\quad - \int_0^x \{B(x')R_1^+(x', 1, s+2(x-x')) \\ &\qquad + \tfrac{1}{2}[A(x')+B(x')](R_1^+ * R_1^+)(x', 1, s+2(x-x')) \\ &\qquad + \tfrac{1}{2}C(c')(1+2*R_1^+ + 1*R_1^+ * R_1^+)(x', 1, s+2(x-x'))\} \, dx'. \end{aligned} \tag{60}$$

Similarly, we can rewrite (21) with $x = 0$ in integrated form as

$$\begin{aligned} R_1^-(0, y, s) &= R_1^-(0, 1, s+2(1-y)) \\ &\quad - \int_y^1 \{B(y')R_1^-(0, y', s+2(y'-y)) \\ &\qquad - \tfrac{1}{2}[A(y')-B(y')](R_1^- * R_1^-)(0, y', s+2(y'-y)) \\ &\qquad + \tfrac{1}{2}C(y')(1+2*R_1^- + 1*R_1^- * R_1^-)(0, y', s+2(y'-y))\} \, dy'. \end{aligned} \tag{61}$$

The first terms on the right-hand side of both the above equations are the known data. Denote them by

$$F^{\pm}(s) \equiv R_1^{\pm}(0, 1, s). \tag{62}$$

Equations (60) and (61) can be used as bases for iterative schemes as follows:

$$\begin{aligned} R_{1,n+1}^+(x, 1, s) &= F^+(s+2x) \\ &\quad - \int_0^x \{B_n(x')R_{1,n}^+(x', 1, s+2(x-x')) \\ &\qquad + \tfrac{1}{2}[A_n(x')+B_n(x')](R_{1,n}^+ * R_{1,n}^+)(x', 1, s+2(x-x')) \\ &\qquad + \tfrac{1}{2}C_n(x')(1+2*R_{1,n}^+ + 1*R_{1,n}^+ * R_{1,n}^+)(x', 1, s+2(x-x'))\} \, dx', \end{aligned} \tag{63}$$

with $0 \leqslant x \leqslant 1$, $0 < s < 2(1-x)$, $n = 1, 2, 3, \ldots$, and

$$\begin{aligned} R_{1,n+1}^-(0, y, s) &= F^-(s+2(1-y)) \\ &\quad - \int_y^1 \{B_n(y')R_{1,n}^-(0, y', s+2(y'-y)) \\ &\qquad - \tfrac{1}{2}[A_n(y')-B_n(y')](R_{1,n}^- * R_{1,n}^-)(0, y', s+2(y'-y)) \\ &\qquad + \tfrac{1}{2}C_n(y')(1+2*R_{1,n}^- + 1*R_{1,n}^- * R_{1,n}^-)(0, y', s+2(y'-y))\} \, dy', \end{aligned} \tag{64}$$

with $0 \leqslant y \leqslant 1$, $0 < s < 2y$, and $n = 1, 2, 3, \ldots$.

The functions A_n, B_n and C_n are given by the initial conditions (18) and (22) according to

$$A_n(x) = 2[R^-_{1,n}(0, x, 0^+) - R^+_{1,n}(x, 1, 0^+)], \tag{65}$$

$$B_n(x) = 2[R^-_{1,n}(0, x, 0^+) + R^+_{1,n}(x, 1, 0^+)], \tag{66}$$

$$C_n(x) = -\kappa^2 c_0^2 l^2 \exp\left[-2\int_0^x A_n(x')\,dx'\right]. \tag{67}$$

Natural choices of starting values for these iterations are

$$R^+_{1,1}(x, 1, s) = F^+(s + 2x), \tag{68}$$

$$R^-_{1,1}(0, y, s) = F^-(s + 2(1 - y)). \tag{69}$$

Sufficient conditions for this iterative scheme to converge are given in [10] for the $C(x) \equiv 0$ case. An analogous consideration can be carried out when $C(x) \not\equiv 0$, but we do not go into further details here. When we have convergence, so that $R^{\pm}_{1,n} \to R^{\pm}_1$, the limits of the left-hand sides of (65) and (66) also exist and thus $A(x)$ and $B(x)$ are obtained (cf. (18) and (22)). The numerical performance of this iterative algorithm is discussed in Section 6.

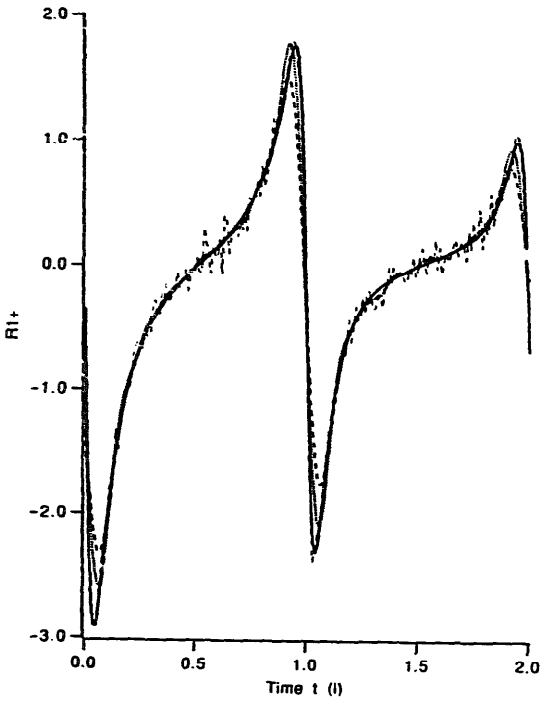

Fig. 3. Restoration of the peaks of R_1^+ after smoothing. The solid line represents the clean R_1^+, obtained from the profile with relative permittivity $\epsilon_r = 4 - 3\cos(40\pi z)$, conductivity $\sigma = 0.02 + 0.01\sin(30\pi z)$ (mho/m) $(0 \leqslant z \leqslant 0.1$ m) and the transform parameter κ (with unit m^{-1}) = 1. The fine dashed line represents the noisy data with rms $S/N = 8.0$. The dashed and dotted lines represent R_1^+ after smoothing the noisy data once without and with restoring, respectively.

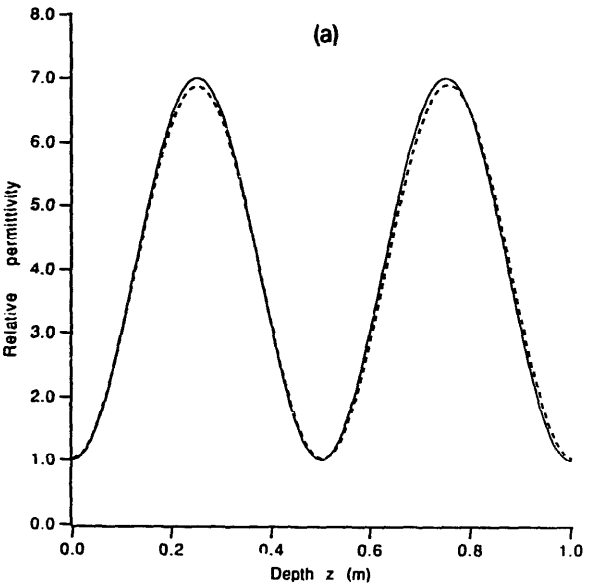

Fig. 4. Reconstruction of permittivity using one round trip data for R_1^+. The conductivity is $\sigma = 0.002 + 0.001 \cdot \sin(3\pi z)$ (mho/m) $(0 \leqslant z \leqslant 1$ m). $\kappa = 1$ m^{-1}. The reconstruction uses 200 data points in (a), (c) and 400 data points in (b), (d).

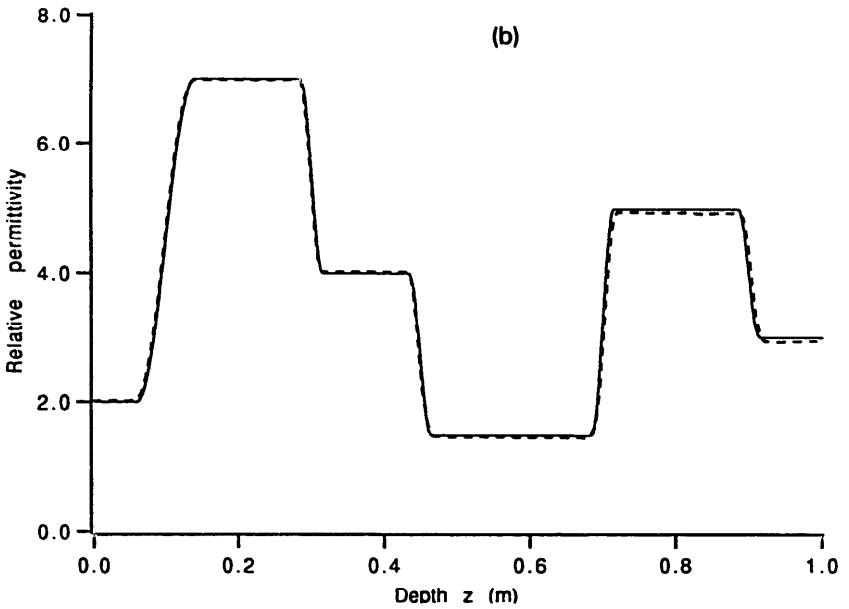

Fig. 4(b).

6. Some numerical examples

The inversion algorithms described in Sections 4 and 5 have been implemented numerically and we present some typical results which are based on clean and noisy synthetic data, respectively. When noise is introduced, it is smoothed by means of a five-point linear

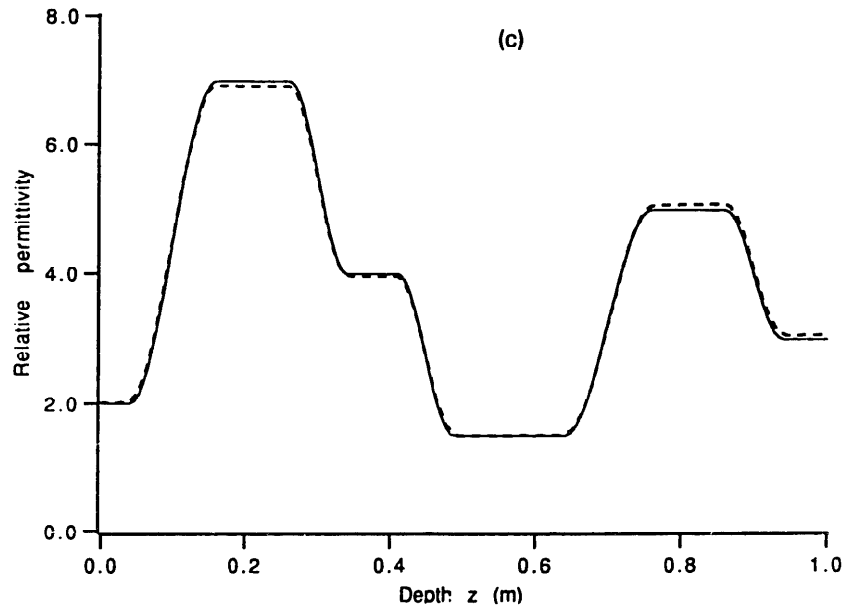

Fig. 4(c).

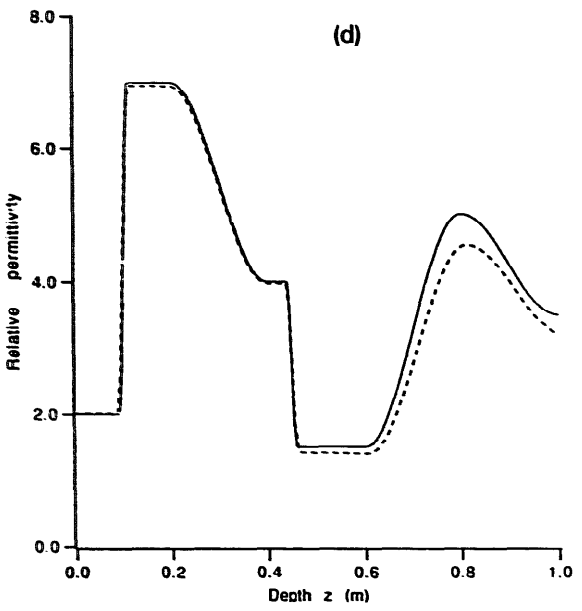

Fig. 4(d).

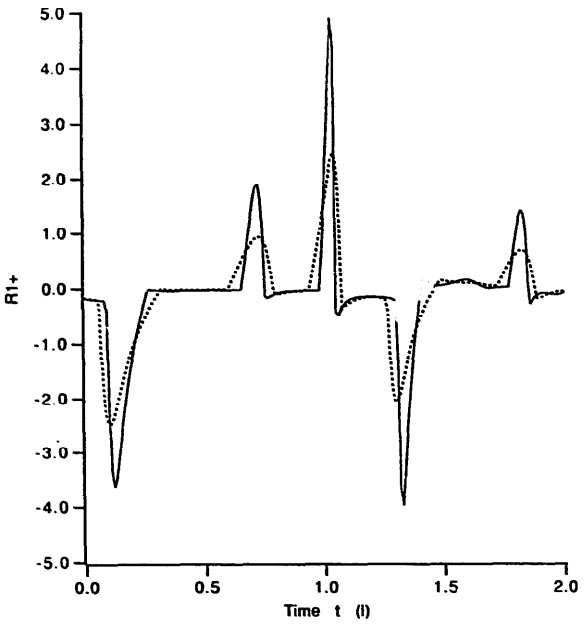

Fig. 5. The $R_1^+(0, 1, s)$ kernel for the the profiles in Figs. 4(b) and 4(c).

least-squares smoother. Sharp peaks will then be smoothed away to a considerable extent. On the other hand, the peaks play a key role in the reconstruction and it has therefore been found necessary to introduce a procedure for restoring the peaks. It has been chosen as follows: the smoother is applied twice and the difference between the first and second smoothing is then added to the result of the first smoothing. The result of this procedure is illustrated on noisy data in Fig. 3. There the solid line is the original data, the fine dashed line is the noisy data with a root mean square signal to noise ratio (rms S/N) of 8.0, the dashed line is the smoothed data, and the dotted line is the "restored" result, obtained as described above. An additional illustration of the effect of restoring the peaks after the smoothing is given in Figs. 6(a) and 6(b) where reconstructions of the permittivity and conductivity using data obtained by smoothing noisy data twice, with or without restoring, are shown.

We note that one-sided data are not sufficient to reconstruct both the permittivity and the conductivity. However, if one of them is assumed to be known, we need only one round trip data $R_1^+(0, 1, s)$, $0 < s < 2$, to reconstruct the other parameter by propagating the boundary values $R_1^+(0, 1, s)$ to the initial condition (18). Figures 4(a)–4(d) illustrate reconstructions of the permittivity in this way. Figure 4(a) shows the reconstruction of a smooth oscillating function $\epsilon(z)$. The inversion algorithm is based on the assumption that $\epsilon(z)$ is continuous. However, it is of interest to investigate how the algorithm works for a rapid variation of $\epsilon(z)$. For profiles with a linear rapid variation of $\epsilon(z)$, it has been found that one needs at least five grid points in each slope region, such as illustrated in Figs. 4(b)–4(d), in order to get reliable reconstructions. Figure 5 shows the $R_1^+(0, 1, s)$ kernel for the profiles in Figs. 4(b) and 4(c). The sharpening of the peaks in R_1^+ associated with a more rapid $\epsilon(z)$ variation is clearly seen here.

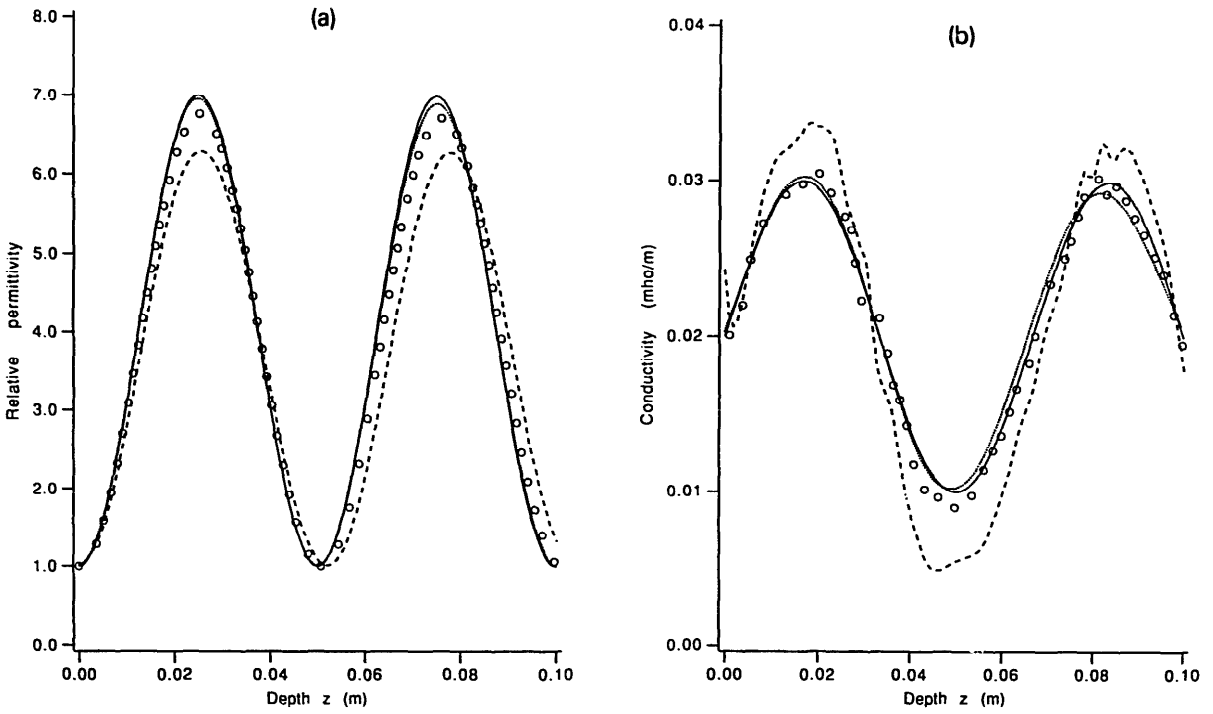

Fig. 6. Simultaneous reconstructions of $\epsilon(z)$ (Fig. 6(a)) and $\sigma(z)$ (Fig. 6(b)) using the inversion algorithm in Section 4. The solid lines are true values. The dotted lines are the reconstructed values using clean data. The dashed lines and circles are reconstructions by smoothing the noisy data twice without and with restoring, respectively (not all circles are displayed). Each reconstruction uses 400 data points. $\kappa = 1\ \mathrm{m}^{-1}$.

Figures 6(a) and 6(b) illustrate the simultaneous reconstruction of $\epsilon(z)$ and $\sigma(z)$ in a model where both are slowly oscillating functions, using the inversion algorithm in Section 4. Reconstructions using noise-free as well as noisy data with rms S/N of 8.0 are shown (uniformly distributed and Gaussian random noise give very similar results). The noisy data have been smoothed and restored using the procedure described above in connection with Fig. 3. Also shown in Figs. 6(a) and 6(b) are the previously mentioned recontructions from data which have been smoothed twice (but not restored).

Figures 7(a)–7(e) illustrate the simultaneous reconstruction of $\epsilon(z)$ and $\sigma(z)$ by means of the iterative inversion algorithm described in Section 5. Figures 7(a)–7(c) show the starting values for the functions $A(x)$, $B(x)$, $C(x)$ (cf. (65)–(69)). As shown in Figs. 7(d) and 7(e), although the initial reconstructions from the values given by (68) and (69) are rather poor, after 20 iterations the reconstructions have improved considerably. After 100 iterations the reconstructions and the true values essentially coincide on the scale of Figs. 7(d) and 7(e).

7. Concluding remarks

In the present paper we have shown that one can formulate the inverse scattering problem for a vertical magnetic dipole field impinging on a stratified slab in such a way that the solution can be obtained using methods and results which are analogous to those available for the case

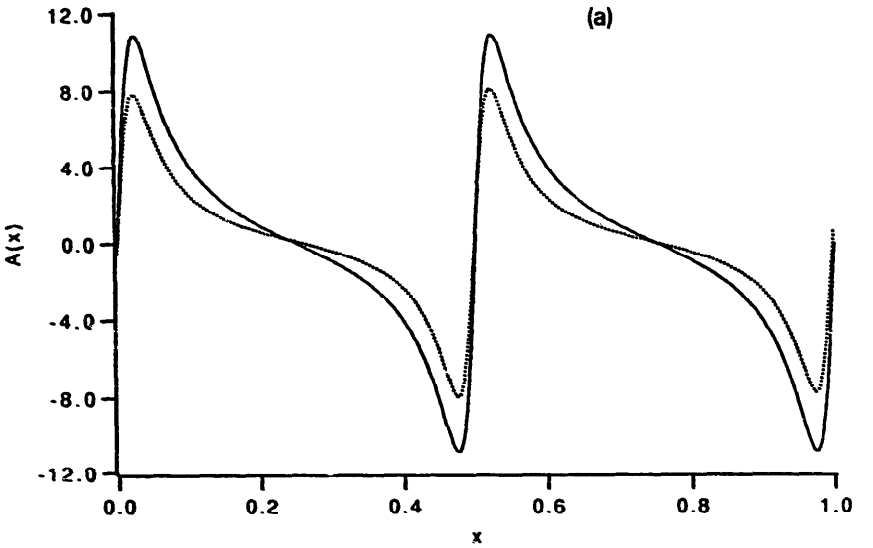

Fig. 7. Simultaneous reconstructions of $\epsilon(z)$ and $\sigma(z)$ using the iterative algorithm in Section 5. The solid lines are true values. The dotted lines are the initial values. The dashed lines in (d) and (e) are the reconstructions after 20 iterations. Each reconstruction uses 400 data points. $\kappa = 1\ \mathrm{m}^{-1}$.

of a normally incident plane wave. However, independent checks of the numerical results are desirable. In this context we note that the extension of the treatment of the dissipative, stratified, half-space scattering problem in [6], by means of the "physical" kernels, to the case of a slab of finite thickness provides one such possibility. The use of the Green functions technique is then of particular interest (cf. [6]).

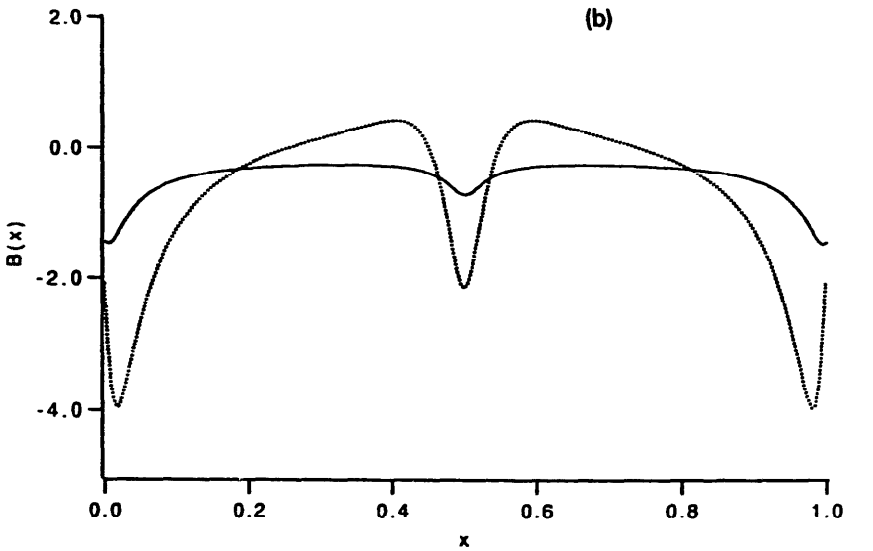

Fig. 7(b).

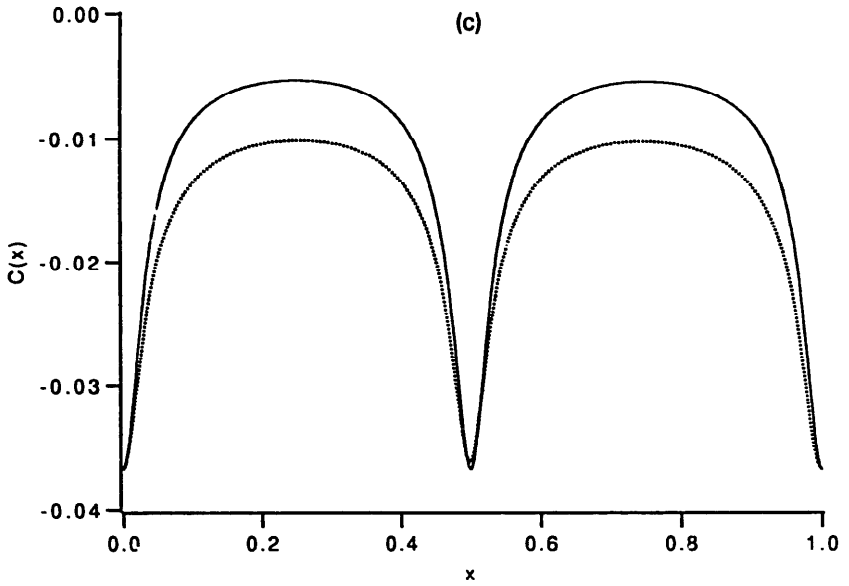

Fig. 7(c).

In the present work and in [6] the splitting is introduced in the free space outside the medium. However, it is also of interest to investigate a formulation based on a splitting inside the dissipative medium and work on this aspect has begun [7].

Furthermore it can be expected that it will be possible (by appropriate modifications; cf. [11,12] in this context) to remove the restriction to permittivity profiles which are continuous at

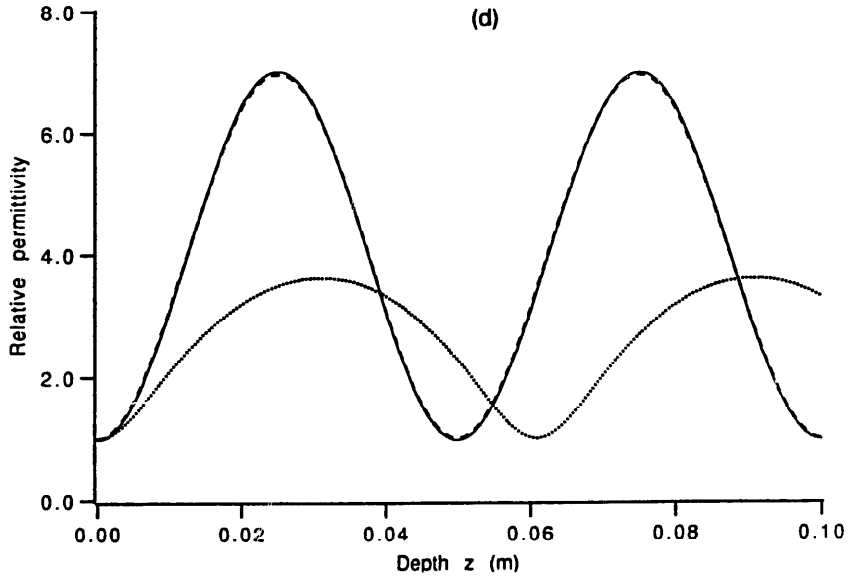

Fig. 7(d).

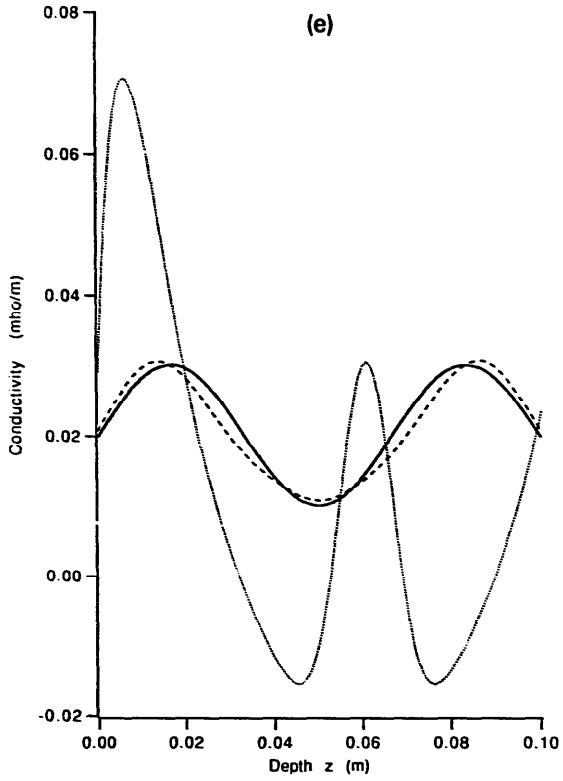

Fig. 7(e).

$z = 0$ and $z = L$. Such a development can be expected to provide the possibility to make comparisons with simple cases with known solutions.

References

[1] R.S. Beezley, Electromagnetic direct and inverse problems for absorbing media, Ph.D. Thesis, Univ. Nebraska, 1985.

[2] J.C. Bolomey, D. Lesselier, C. Pichot and W. Tabbara, Spectral and time domain approaches to some inverse scattering problems, *IEEE Trans. Antennas and Propagation* **AP-29** (1981) 206–212.

[3] J.P. Corones, M.E. Davison and R.J. Krueger, Wave splitting, invariant imbedding and inverse scattering, in: A.J. Devaney, Ed., *Inverse Optics*, Proc. SPIE **413** (SPIE, Bellingham, WA, 1983) 102–106.

[4] J.P. Corones, M.E. Davison and R.J. Krueger, The effects of dissipation in one-dimension inverse problems, in: A.J. Devaney, Ed., *Inverse Optics*, Proc. SPIE **413** (SPIE, Bellingham, WA, 1983) 107–114.

[5] J.P. Corones and R.J. Krueger, Obtaining scattering kernels using invariant imbeding, *J. Math. Anal. Appl.* **95** (1983) 393–415.

[6] S. He and A. Karlsson, Time domain Green functions technique for a point source over a dissipative stratified half-space. Technical Report TRITA-TET 91-1, Royal Institute of Technology, Stockholm, 1991.

[7] S. He, Factorization of a dissipative wave equation and the Green functions technique for axially symmetric fields in a stratified slab, *J. Math. Phys.* **33** (3) (1992) 953–966.

[8] S. He and S. Ström, The electromagnetic scattering problem in the time domain for a dissipative slab and a point source using invariant imbedding, *J. Math. Phys.* **32** (12) (1991) 3529–3539.

[9] G. Kristensson and R.J. Krueger, Direct and inverse scattering in the time domain for a dissipative wave equation. Part I, Scattering operators, *J. Math. Phys.* **27** (1986) 1667–1682.
[10] G. Kristensson and R.J. Krueger, Direct and inverse scattering in the time domain for a dissipative wave equation. Part II. Simultaneous reconstruction of dissipation and phase velocity profiles, *J. Math. Phys.* **27** (1986) 1683–1693.
[11] G. Kristensson and R.J. Krueger, Direct and inverse scattering in the time domain for a dissipative wave equation. Part III. Scattering operators in the presence of a phase velocity mismatch, *J. Math. Phys.* **28** (1987) 360–370.
[12] G. Kristensson and R.J. Krueger, Direct and inverse scattering in the time domain for a dissipative wave equation. Part 4. Use of phase velocity mismatches to simplify inversions, *Inverse Problems* **5** (1989) 375–388.
[13] R.J. Krueger, An inverse problem for a dissipative hyperbolic equation with discontinuous coefficients, *Quart. Appl. Math.* **34** (1976) 129–147.
[14] R.J. Krueger, Numerical aspects of a dissipative inverse problem, *IEEE Trans. Antennas and Propagation* **AP-29** (1981) 253–261.
[15] V.H. Weston, Factorization of the wave equation in higher dimensions, *J. Math. Phys.* **28** (5) (1987) 1061–1068.
[16] A.E. Yagle, One-dimensional inverse scattering problems: an asymmetric two-component wave system framework, *Inverse Problems* **5** (1989) 641–666.
[17] A.E. Yagle and B.C. Levy, A fast algorithm solution of the inverse problem for a layered acoustic medium probed by spherical harmonic waves, *Geophys. J. Roy. Astr. Soc.* **78** (1985) 729–737.